SETTING UP OF A COST-EFFECTIVE CONTINUOUS DESALINATION PLANT BASED ON COUPLING SOLAR AND GEOTHERMAL ENERGY

[1]Farnè Stefano, [2]Giovenzana Valentina*, [2]Beghi Roberto, [3]Lavanga Vito, [2]Guidetti Riccardo

*corresponding Author: valentina.giovenzana@unimi.it

[1]University of Pavia - Department of Industrial, Electrical, Computer and Biomedical Engineering

[2]Department of Agricultural and Environmental Sciences - Production, Landscape, Agroenergy

[3]Freelance researcher and inventor

Abstract.

The aim of the work was to describe and test a solar desalination system for salt and brackish water desalination considering a real application, in order to provide detailed technical features of a future plant based on the calculated data by the modelling approach. The main innovative aspect of the studied solar desalination system consists in reproducing, in a restricted environment, the water cycle that commonly occurs in nature. The process is a thermal distillation process based on a first humidification phase and a second phase of air dehumidification, exploiting, at steady-state conditions, only solar thermal energy, and it is capable to work 24 h day^{-1}. It is built with materials that are commonly used in the building sector, reducing construction costs. The findings have led to a system easily integrable in real scale scenarios to recover fresh water from a solution of salt or brackish water, for both potable uses and process uses. Thanks to these technological solutions, a low specific energy consumption (5.5 kWh m^{-3} of water) is obtained, envisaging lower running cost.

Keywords. *solar power, geothermal energy, potable water, energy savings, functioning model*

1. INTRODUCTION

The desalination of seawater is characterized by a wide use of fossil energy sources, with a considerable environmental impact. Traditional evaporative plants are based on the evaporation of saltwater and the subsequent condensation of humidified air using thermal or electric energy through conventional sources. To date, around the world, to produce 1000 m^3 d^{-1} of fresh water for 10 ktoe y^{-1} multiples of the tons of oil equivalent, it is more usual to speak of millions of tons of oil equivalent and kilotons of oil equivalent (ktoe) are necessary, and that is why in recent years new systems powered by renewable sources have taken hold.

There are several possible desalination processes. Membrane processes create a separation between two fluids by applying a driving force to a selective barrier that is permeable only by some of the substances present in the fluid. The different types of processes are discriminated according to the source that produces the driving force: electrodialysis (exploits the action of an electric field), filtration (exploits a pressure gradient), osmosis (exploits the chemical potential), or dialysis (exploits the concentration gradient). Among these, the most commonly applied in the desalination process is reverse osmosis (RO) (Nam et al., 2011), obtained in recent years by using renewable sources, as in the case of the Italian Lampedusa plant (Tzen et al., 2012): capable to provide 120 m^3d^{-1} of desalinated water through two RO units and the supply of electricity takes place via a 100 kW_p photovoltaic plant equipped with accumulation systems. The specific consumption is 5.5 kWh m^{-3} of desalinated water produced. Incoming water is pretreated through filtration and chemical substances, to prevent fouling and corrosion. Salt content in the obtained water is lower than 500 ppm, in compliance with the drinking water specifications of the World Health Organization (WHO, 2017; Rognoni, 2010).

Over the years an evolution of desalination systems has been seen in term of efficiency (Ayoub and Malaeb, 2014; El-Agouz, et al., 2014; Kang, et al., 2014; Park et al., 2012) and using renewable energy sources (Qiblawey and Banat, 2008; Salata and Coppi, 2014) as efficient solution for scarcity of water

and electricity (Kabeel et al., 2014). The most used sources in desalination are solar, wind and geothermal. Among these, the solar energy plays a particularly important role because it accounts for 57% of energy production for water desalination (Reddy & Sharon, 2014). The solar energy-based systems become competitive where there is a large availability of renewable sources. In the more recent systems, a portion of the total energy is supplied by a solar energy system (table 1), thus constituting a hybrid system (Cipollina et al., 2009; Rognoni, 2010). Multistage flash (MSF) and Multiple Effect Distillation (MED or ME) are the evaporative technologies most frequently used, where in some cases solar technology has also joined (Tzen et al., 2012). Bacha in 2013, Nematollahi et al. in 2013, and Hamed et al. in 2014 provided mathematical and experimental investigation of solar desalination systems. Experimental study on solar desalination system based on humidification and dehumidification process were performed by using solar air heater with evacuated tubes (Li et al., 2014) and by using a novel multi-effect (Chang et al., 2014).

An innovative system for salt and brackish water desalination is presented in this paper, the technology is almost totally exploiting solar power and capable of producing distilled water with very low running costs if compared to current technologies. The objective of this paper is to describe and test the innovative solar desalination plant considering a real application, in order to define a functioning model of the plant itself, and a possible designing. The final aim is to provide detailed technical features of a future plant based on the calculated data by the modelling approach.

2. MATERIALS AND METHODS

2.1 DESCRIPTION OF THE PLANT

The innovative solar desalination named SDGC (Solar Desalination Geothermal assisted Continuous) is an innovative thermal distillation process essentially based on a first humidification phase and a second phase of air dehumidification, exploiting, at steady state, only solar thermal energy (Figure 1).

Geothermal assistance is a strategic solution to operate in extreme conditions, e.g. for energy supplies (in cold climates), mainly to interrupt situations of stall/balance at sustained thermal regimes, being capable to create gradients to keep the plant running and to maintain tropical convective dynamics.

Development of this process is based on achieving a condition of equilibrium in which the only energy necessary for the system is provided to compensate the inevitable inefficiencies, thus allowing the process of self-maintenance for a sufficiently long time to justify its industrial use. The system is made up of a parallelepiped concrete tank thermally insulated by polyurethane foam panels. The inside is filled to about two thirds of the volume with the saltwater to be treated. In correspondence with the free surface of the plant, the tank is crossed by a series of corrugated pipes, made of materials characterized by a high thermal conductivity and connected to the system that will provide the main thermal energy and maintenance energy that will heat the salt water and maintain it at the established regimes. Other corrugated pipes of the same material run through the tank at the top, bottom and side of the system; the function of reserve heat exchangers, able to intervene if a thermal equilibrium condition is reached in the system which represents a critical feature of the plant operation.

The whole tank is longitudinally crossed by a set of pressed sheets made of a material of high thermal conductivity and has an appropriate size and a predetermined percentage of vacuum/solid, such as to optimize the need for a sufficiently extended heat exchange surface while not hindering the movement of air. These plates are installed vertically in the central part of the tank, while they open to an accordion-like structure in the upper and lower part (Figure 2).

Near the free surface and up to a certain depth in the salt water, these sheets are compacted and thermally insulated with respect to the portion of water heated by the main heat exchanger, and the interstices formed by the reciprocal tiling are filled with liquid aluminum (Lavanga and Farné, 2017).

In order to allow the process to develop with sufficient industrial speed, the whole tank is kept depressurized.

2.2 MATERIALS USED

Reinforced concrete tanks were chosen, as commonly used in water treatment plants. For the case study, a 50 m^3 capacity reinforced concrete tanks was chosen (model C-15, Gazebo S.p.A., Gatteo, FC, Italy).

Foam panels characterized by thickness 100 mm, thermal transmittance 0.23 W m^{-2} K^{-1}, operating range -40°C to 110 °C were chosen (GT model, Stiferite S.r.l., Padova, Italy). It has been chosen to install two superimposed panels of a total thickness of 200 mm.

It was decided to use corrugated copper pipes, in order to guarantee an adequate degree of turbulence in the heat-carrying fluid and therefore to promote heat exchange. These pipes are produced by the company Pantani Divisione Tubi S.r.l.

In addition to the above reasons, it is thought that due to the turbulence inside the corrugated piping micro-vibrations are created which, when transmitted to the water, promote its evaporation.

For the case study, an expanded metal (aluminum; 1000 x 2000 mm; thickness 2 mm) with rhomboidal mesh was chosen, produced by the company Fratelli Mariani S.p.A. and having carving measures of 62 x 20 mm and open area 30 %.

Near the free surface, the pressed sheet metal side by side must constitute a region with a high thermal conductivity that can dispose of the heat in an efficient way, so as to allow a sufficiently rapid condensation process. To guarantee this function, near the free surface, the sheets will be separated from the saltwater through polyurethane foam panels (coated with aluminum to protect against salt corrosion) forming a compact sheet packet. To fill the interstices that will inevitably be formed in the package of sheet metal side by side, it will be injected liquid aluminum inside the structure.

To achieve adequate process speeds, it is necessary that the convective motions developed inside the tank are characterized by a rather high speed, to push the evaporation and condensation phases to the maximum.

To obtain this result it is possible to use tangential stirring systems powered by electric motors. In the future it will be possible to evaluate the feasibility of using the patented Mixer Homogeneous in Local Media (MHLM^{TM}) mixing system (Lavanga and Farné, 2016).

2.3 Operating conditions

After some preliminary calculations (data not shown), a good level of productivity was achieved through the implementation of the measures work in vacuo, artificial movement of indoor air, adequate operating temperatures, adequate evaporating surface, and transversal and longitudinal gradients. Table 2 shows the operating conditions considered.

For this study, it was assumed that the tank was installed on a ground support, in the Milan area, where the average annual temperature is about 13°C.

Table 3 shows the result of the calculations performed. Limiting coefficient of water was obtained from (Calza, 2010).

The total evaporating surface is divided in half by the presence of the thermal tunnel, both halves operating under the same operating conditions; this allowed us to perform the calculation on one of the two halves of the tank and then extend it to the entire evaporating surface. Table 4 shows the total water flow and the power transmitted to the air through latent heat.

Thermophysical parameters used have been obtained from tables showing the air properties (Moran et al., 2011; Magrini and Magnani, 2009).

Binary diffusivity was obtained from suitable diagrams in conditions of pressure and temperature equal to 101325 Pa and 300 K; to bring it back to the process conditions, the following formula was applied, remembering that the binary diffusivity of the perfect gases is approximately proportional to the relation:

$$D_{AB} = D_{AB(300K;1atm)} \left(\frac{P}{P_{ex}}\right)\left(\frac{T_{ex}}{T}\right)^{1.75} \qquad \left[\frac{m^2}{s}\right] \qquad (1)$$

Where

P_{ex} and T_{ex} represent the pressure and operating temperature, expressed in atmospheres and Kelvin (Clarkson, 1998).

The value of the latent heat was evaluated at the working pressure through the aforementioned tables; in order to bring it back to the temperature conditions of the system, the Watson correlation was exploited (Pantani, 2010):

$$r_{p,t_{ex}} = r_{p_{ex}} \left(\frac{T_c - T_{ex}}{T_c - T_{eb}}\right)^{0.38} \qquad \left[\frac{kJ}{kg}\right] \qquad (2)$$

where:

$r_{p,t\,ex}$ [kJ*kg^{-1}]: latent heat of vaporization at working pressure;

T_c [K]: critical temperature, equal to 647 K;

T_{eb} [K]: boiling temperature at operating pressure conditions, equal to 342.25 K (69.1°C).

With the conditions of speed, pressure and temperature adopted, it is possible to push the system up to a daily production of approximately 4000 kg d^{-1} of evaporated water. This will be the maximum condensable amount in the system.

The peculiarity of this process lies in the possibility of fully recovering the latent heat of vaporization, quantified in a power value of approximately 110 kW.

The preliminary evaluation of the heat exchange was performed by putting in conservative conditions and carrying out the calculation assuming the use of a smooth tube. In the tank there will be two exchangers of this type, one placed in each half of the tank, and both return flow connections will be connected to the heat generators through two suitable hydraulic manifolds. Table 5 shows the summary of the calculations.

To calculate the amount of condensate produced, it is necessary to know the thermo-hygrometric conditions of the humid air inside the tank before and after condensation and to know the dry air flow to determine the sizing power of the exchangers. Table 6 shows the results of applying the model.

To be capable to condense the same amount of water that evaporates, it is necessary to create an exchange surface that allows the absorption of a thermal power equal to 116.95 kW.

The expanded sheets, in addition to have the proper thermal properties to be used for the purpose, must also have mechanical characteristics such as to make it an excellent support on which the condensed water can adhere.

The disposition of the expanded metal sheets must be made in such a way as to minimize the interference between adjacent sheets, maximizing the interaction between the fluid and the exchange surface. Moreover, the opening of the expanded metal sheets in the upper part of the system must be made in such a way that the minimum inclination of the plate with respect to the horizontal enables the adhesion forces to allow the condensate drop to adhere to the metal surface and to percolate towards the collection system, avoiding it falling into the tank. For the preliminary dimensioning, it was preferred to obtain the value of the maximum inclination angle experimentally, observing the behavior of a drop of water in contact with an aluminum surface inclined with ever increasing slopes. The result shows that, to ensure the rapid disposal of condensate drops, preventing them from being detached, the outer sheets must form an angle of no less than approximately 50°. Below this value it has been observed that the drop speed of the drops decreases, causing an increase of mass and the consequent detachment from the contact surface. Table 7 shows the sizing of the thermal tunnel.

The base of the thermal tunnel is a region with high thermal conductivity and is in direct contact with the colder water at the bottom of the tank. Therefore, its temperature has been hypothesized not to be much higher than that at the bottom. In order to avoid the heat developed by the main heat exchanger being transmitted to the expanded sheets, disturbing the absorption of thermal energy

during condensation, the insulation panels of the thermal tunnel will be extended beyond the base for a certain length, which will be established during the project execution. This extension is thought to lead to a significant reduction in the convective heat exchange coefficient between the base of the thermal tunnel and the air to be dehumidified. Therefore, to consider this phenomenon, a reduction of 30% was considered.

Explained in the previous section, the SDGC system is designed to be capable to self-maintain when brought to operating temperatures. For this purpose, it was decided to use two different heat generators:

Solar thermal system: this operates mainly under the regime conditions in order to reintegrate the heat losses through the enclosure;

Heat pump system: this operates mainly at start-up, in order to bring saltwater from the feed from the conditions in the tank up to the average operating temperature.

However, while the two plants can work in synergy to reduce the start-up times, solar thermal will be the primary generator once the SDGC system has reached full capacity.

For the case study, the use of vacuum solar collectors was chosen because of their ability to bring the water to high temperatures, in harmony with those of operating the plant. The type of collector chosen for sizing is the Sky Pro 18 model produced by the company Kloben Industries S.r.l, having the characteristics of interest shown in Table 8.

The sizing of the collectors was carried out assuming installation of the plant in Milan and considering the operating system for 8000 h y^{-1}. To obtain a datum concerning the minimum number of collectors necessary, it was decided to calculate the global radiation assuming installation of the collector in the best possible operating conditions, which translates into geographic orientation in the SOUTH direction (azimuth equal to 0°), angle of inclination on the horizontal optimal for the operation of solar panels (35°), absence of shadowing and obstacles.

211 Under these assumptions, the operational efficiency of the collector was calculated using the following
212 formula (Battisti, 2013):

$$\eta = \eta_o - \frac{k_1}{I}\Delta T - \frac{k_2}{I}\Delta T^2 \qquad [\%] \qquad (3)$$

where:

213 η_o [%]: optical efficiency of the collector.

214 k_1, k_2 [W*(m^{-2} K^{-1}]): thermal dispersion coefficients.

215 ΔT [K °C]: difference between the average temperature inside the collector and the external
216 environment;

217 I[W/(m^{-2}]): effective irradiation on the collector.

218 Table 9 shows the sizing of solar collectors.

219 For the case study it was therefore decided to use a water/water heat pump (P.D.C.), in which the
220 evaporator is in communication with a thermo-well, T.P. (Lavanga and Sparacino, 2013).

221 The calculations for the case study were made considering the Vitocal 300-G heat pump, model WW
222 301.A21, produced by the company Viessmann GmbH. Table 10 shows the main operating data.

223 For a first analysis we chose to operate conditions W10/W55. In this way the saltwater will be brought
224 to the temperature of 55°C and the solar thermal plant will be responsible for compensating the small
225 temperature difference between the heat pump regime and the average operating temperature. It
226 was decided to operate in this way to avoid a too high penalty on the coefficient of performance COP.
227 Table 11 shows the operating conditions of heat pump generator.

228 In the calculation, the volume (and consequently the mass) of saltwater to be heated was considered
229 equal to 30% of the whole saltwater mass inside the tank, because the objective is to heat only the
230 portion of fluid near the free surface. Figure 3 shows a diagram of the layout of the SDGC plant with
231 the heat generators: solar thermal (S.T.), heat pump (P.D.C.) and thermo-well (T.P.).

3. RESULTS AND DISCUSSION

The operating principle is based on heating only the saltwater close to the free surface, while that on the bottom remains at a lower temperature. During the steady state operation, the free surface of the saltwater is maintained at an average temperature of 55-60 °C by the solar thermal system, while at the bottom remains at around 15-25 °C (the temperature of the water entering the tank). This transverse temperature gradient recalls the principle of operation of the stratified storage systems used in thermo-hydraulic systems and is of fundamental importance for the operation of SDGC, because it represents the real "engine" of the system. The point of introduction of thermal energy is not accidental; the flow of the heating system, in fact, is in the central part of the system (Figure 2, arrows pointing up), while the return is positioned near the walls of the tank. This makes it possible to obtain a non-homogeneous temperature distribution at the free surface and promotes the trigger and maintenance of the convective rotational motions. The arrangement of the horizontal exchangers and their feeding predispose high horizontal gradients, favoring horizontal laminar flows towards the center, generating rotary/convective motions in the aerial phases; the lateral vertical exchangers (immersed), with the set gradients, favor the convective motions that feed the rotary/convective motions in the liquid phases (suitably triggered to break situations of balance).

The upper part of figure 2 shows the movement of moist air (in the right quadrant with a clockwise rotation, while in the left quadrant with a counterclockwise rotation); warm air, more humid, is represented with a red semicircle, while cold air, less humid, is represented with a blue semicircle.

On the free surface of the tank, an evaporation process begins which, unlike boiling, has a lower speed and affects only the free surface of a fluid mass, as well as being visible at any temperature. Together with evaporation, on the free surface there is also a transfer of heat from the water to the air that allows the triggering of convective motions, promoted by the agitation system inside the tank. The greatest evaporation occurs near the central part of the system, due to the higher delivery

temperature and, thanks to this, the air is charged with humidity. Furthermore, the vacuum setting of the tank further increases the evaporated flow rate. The heated and humidified air, pushed upwards by convective motions (the circles of the upper part of figure 2) and by the stirring system, encounters the expanded metal sheets of the accordion shaped structure. These metal sheets, being in direct contact with the colder water at the bottom of the tank, are characterized by a temperature lower than the dew point temperature of the moist air; so, in this phase, the dehumidification process takes place by condensing the water vapor in contact with the metal sheets. The condensate percolates on the expanded metal sheets up to a collection channel, to be sent outside the plant.

No systemic supply of air is expected, except for maintaining desired pressure/depressor regimes for specific programmed regimes. The "expanded metal", continuous or set up with two symmetrical intercalated packs (for practical implementation), in the intermediate part form the compact/continuous central body (with high thermal conductivity), which together with the two external insulating bodies forms the "thermal tunnel". It allows high condensation temperatures to flow downwards and be transferred to the colder layers of liquid, which by heating feed the rotary/convective motion that brings them to the surface, feeding the dynamic cycle.

The condensation heat transferred to the expanded metal is totally conveyed to the layers of liquid at lower temperatures, considering the absence of possibilities for leaks from the entire system (adiabatic as a whole).

In this phase the humid air gives heat to the sheets, which also includes the latent heat of condensation. Thanks to the thermal gradient between the upper part of the sheets, which is warmer due to dehumidification, and the lower part immersed in the cold salty water, the absorbed heat is conveyed towards the lower part of the system through the “thermal tunnel” (figure 2, the arrow pointing down), where it is transmitted to the salt water (shown in the lower part of figure 2 by the horizontal arrows, facing right and left in the respective quadrants) and then recovered. This heat

transfer triggers convective motions inside the liquid mass; these motions are represented by the circles in the lower part of figure 2 (the semicircle represents the ascending current, by virtue of the higher temperature, while the blue semicircle represents the descending, colder current). Figure 2 shows the convective motions and the energy flows involved in the system which reproduces, obviously on a much smaller scale, the motions and the exchanges between the oceans and the atmosphere, especially at the Earth's equator. As the humidified air gives up heat during the condensation phase, its temperature continues to decrease to a point where it has reached a condition that causes it to move downwards. Considering the submerged portion of the system, as described before, convective motions are formed: the heat given off by the sheets, in fact, heats the water at the bottom of the tank, which, thanks to the different density, rises back to the free surface, producing convective motions.

By virtue of the foregoing, the efficiency of the system is evident; in fact, unlike conventional systems, thanks to the maintenance of temperature gradients and the vacuum at the preset values, by supplying the initial thermal energy at the start of the process, the plant is capable to sustain itself autonomously through the total recovery of latent condensation heat, integrating only the energy necessary to compensate for losses through the enclosure (Lavanga and Farné, 2017).

3.1 CRITICAL FUNCTIONING

The worst condition is reached when the thermal gradients are reset and the tank is all at the same temperature; in this case, the evaporation stops, and the heat cannot circulate through the thermal tunnel. In this case it is necessary to break the thermal equilibrium, re-establishing the right gradients so that the system resumes operation. To this end, auxiliary safety exchangers are installed that can transfer the thermal energy from one area of the tank to another or transfer it to the thermocouple in the event of excess. These exchangers must be capable to restart the system as soon as possible, so they must be capable to transfer a large amount of heat in a short time. In the first analysis it was

assumed to install a piping circuit passing between the upper and lower part of the tank, filled with a heat-carrying fluid (water or other better performing fluids). With the aid of a hydraulic pump, the movement of the fluid would allow the absorption of thermal energy from the humidified air to transfer it to the colder water at the bottom of the tank. In this way, the thermal tunnel would be able to dispose of the remaining thermal energy without the risk of reaching the thermal equilibrium between the humidified air and expanded sheets. The calculation shown in Table 12 follows the calculation principles dictated by technical physics (Magrini & Magnani, 2009), in which some parameters have been set:

- The temperature of the thermal fluid inlet and outlet from the pipeline, on which the thermophysical parameters necessary for the calculation depend;
- The dimensions and material of the piping, referred to standardized industrial products.
- The internal speed in the piping.

By installing 15 pipes connected in parallel through a suitable collector, the system is capable to absorb a quantity of heat equal to about 40% of the total to be disposed of through the thermal tunnel, enough to restart the process in the event of a system stall.

The worst criticality for the operation of the system is represented by the zeroing of the thermal gradients. This situation can occur for two main reasons: in the system, insufficient thermal energy was introduced to compensate for losses through the enclosure and to guarantee the formation of thermal gradients suitable for making the system work efficiently. Too much thermal energy was introduced into the system, saturating the system and bringing the tank to the same temperature at each point. While in the first case it is sufficient to introduce further thermal energy, the second case certainly deserves more attention. It may be due to malfunctions or to unsuitable control systems. In any case, if this situation occurs, the tank being well insulated and therefore with limited losses, it is

necessary to withdraw a portion of this thermal energy and transfer it outside the system in order to restore the thermal gradients necessary to restart the process. For this purpose, it was decided to install a series of pipes along the side walls of the tank, similar to the solution adopted in the previous paragraph, in which a heat-carrying fluid is circulated to absorb thermal energy from the salt water and transport it outwards, to be dissipated in the environment or stored in a thermal storage system. In this way, the cooling of the saltwater will allow the thermal tunnel to start the condensation process again. Table 13 shows the calculations performed for sizing. By installing six exchangers in parallel close to the sidewalls of the tank, they will be able to absorb about 380 kW of thermal power. This power will be sufficient to break the thermal equilibrium by bringing the system to work again in a time of about 3 h. Table 14 gives a verification calculation. Once the sizing of the main elements of the system has been completed, figure 4 shows the dimensioned drawing of the SDGC system.

3.2 System innovation

The SDGC system was found to be a potential alternative to traditional plants. The main innovative aspect of the system consists in reproducing, in a restricted environment, the water cycle that commonly occurs in nature. In fact, through the solar thermal energy, part of the water present in the seas and oceans evaporates according to the relationship presented in paragraph 2.2, returning towards the atmosphere. Thanks to the convective motions, the mass of water in the aeriform state is pushed up to an environment in which it condenses, thanks to the low pressures and temperatures, precipitating successively to the ground. The SDGC system exploits and accelerates this process: solar energy is used to heat the heat-carrying fluid which, by means of a heat exchanger, heats the surface of the mass of water present in the tank, making it evaporate in a closed environment in vacuum and with artificially accelerated moist air. All this allows a faster process and the almost total recovery of latent heat thanks to the presence of the thermal tunnel. In Table 15 it is shown a first positive comparison between the unit module and the orders of magnitude of the current technology park.

In this section, it showed the comparison between the system sized in the case study and some plants, operational and experimental, set up for the exclusive operation of solar energy, with the aim of highlighting the additional innovative and technological features of the SDGC system. Table 16 shows the declared data of the plants under examination, obtained from analysis of the scientific literature. From this comparison, it can be deduced that the SDGC system, with a production level comparable to MED and RO plants powered by solar energy, investment costs, presents significantly lower production costs and specific consumption. This is due to the simplicity of construction that characterizes the SDGC system; exploiting standard commonly used products reduces the costs associated with the development of new elements, which would certainly lead to an increase in the total investment cost. The modular nature of the system also allows the system to be rescaled according to the production size without completely redesigning the system, thus guaranteeing a reduced design cost.

The operation of the system allows the recovery and continuous reuse of the latent heat, making the SDGC a practically self-supplying system, since the thermal energy supplied during the start-up phase is continuously reused thanks to the presence of the thermal tunnel, unless lost through the envelope, which is reintegrated through solar collectors. This element represents the heart of the whole system and at the same time its most delicate part. In fact, it plays a dual role of equal importance: acting as a condensation and condensate collection surface and at the same time recovering the latent heat to reuse it within the system itself, allowing it to self-feed. This second function is implemented by realizing a communication path, using the procedure described in the previous sections, between the condensation zone and the exchange zone at the bottom of the tank, passing through the portion of water heated to the free surface. This solution, which in the first analysis seems simple, represents a great innovation, since it allows the complete recovery of the latent heat to feed the main process and not, as often happens in traditional systems, for secondary pre-heating functions. This allows a drastic

reduction of the energy to be supplied to the system and, consequently, the related costs.

Thanks to these technological solutions, a specific consumption of energy is obtained that is much lower than that of the plants shown in Table 15 and allows a much lower production cost compared to alternative plants. This makes the SDGC system competitive, even with a higher investment cost, because, as shown it allows a return of the investment cost in a sufficiently short time, relative to the average life of this type of plant.

Overall, desalination processes are characterized by a negative environment impact due to their intensive consumption of energy and brine disposal. Using renewable energy to desalination processes will mitigate some of this impact, although the current water production cost from renewable-energy-coupled desalination systems is much higher than the water cost of conventional desalination systems (Al-Karaghouli & Kazmerski, 2013). The results obtained have therefore found in the studied system a possible alternative to the desalination methods present on the market today, thanks to a low specific consumption of energy allowing a return of the investment cost in a sufficiently short time, relative to the average life of this type of plant. Regarding the technical-economic optimization, the first sizing considers only the effectiveness and standardization of the inserted elements, for the future development it will be necessary to optimize all the elements for a significant reduction of the installation cost leading to a remarkable decrease of the cost of water produced. The model presented represents a reliable method to describe the functioning and allow an initial sizing of the plant.

4. CONCLUSIONS

An innovative system for salt and brackish water desalination, Solar Desalination Geothermal assisted Continuous (SDGC), covered by an Italian patent, was described and tested considering a real application. Physical structure of the plant was recalled along with the principle underlying its operation; later, the first model of calculation of the system was introduced, one of the main subjects

of this paper. The analysis model made it possible to relate the geometrical and thermophysical parameters to the operating conditions of the plant, allowing a simple and easy-to-use formulation to be obtained for calculating the producibility of the plant. Based on the calculation model, it was possible to make a preliminary sizing of the most important parts, assessing any critical operating conditions and preparing the most suitable systems to counteract them. During this development phase, particular attention was paid to the standardization of the system, choosing to assemble elements commonly available in the commercial sector of the industrial sector, paying more attention to the functionality and effectiveness of the element and leaving the system optimization for future development in relation to the choice of using products and materials made to measure for a specific function. The result has led to the determination of a standard module, characterized by a good level of producibility in terms of condensed water, which could be appropriately replicated to obtain the level of productivity sought by a possible customer. The SDGC system was found to be a potential alternative to traditional plants.

Thanks to these technological solutions, a low specific energy consumption is obtained and allows a much lower production cost compared to alternative plants. This makes the SDGC system competitive, even with a higher investment cost, because, as shown it allows a return of the investment cost in a sufficiently short time, relative to the average life of this type of plant.

REFERENCES

Al-Karaghouli, A., & Kazmerski, L. L. (2013). Energy consumption and water production cost of conventional and renewable-energy-powered desalination processes. Renewable and Sustainable

Energy Reviews, 24, 343-356. https://doi.org/10.1016/j.rser.2012.12.064

Ayoub, G. M., Malaeb, L. (2014). Economic feasibility of a solar still desalination system with enhanced productivity. *Desalination*, 335(1), 27-32. https://doi.org/10.1016/j.desal.2013.12.010

Bacha, B. H. (2013). Dynamic modeling and experimental validation of a water desalination prototype by solar energy using humidification-dehumidification process. *Desalination*, 332, 182-208. https://doi.org/10.1016/j.desal.2013.05.011

Battisti, R. (2013). *Impianti solari termici per reti di teleriscaldamento*, Dario Flaccovio, Palermo.

Calza, F. (2010). *Manuale degli impianti termici e idrici*, Tecniche Nuove, Milano.

Chang, Z., Zheng, H., Yang, Y., Su, Y., Duan, Z. (2014). Experimental investigation of a novel multi-effect solar desalination system based on humidification-dehumidification process. *Renewable Energy*, 69, 253-259. https://doi.org/10.1016/j.renene.2014.03.048

Cipollina, A., Micale, G., Rizzuti, L. (2009). *Seawater Desalination: Conventional and renewable energy processes*. New York: Springer.

El-Agouz, S. A., Abd El-Aziz, G. B., Awad, A. M. (2014). Solar desalination system using spray evaporation. *Energy*, 76, 276-283. https://doi.org/10.1016/j.energy.2014.08.009

Hamed, M., Kabel, A., Omara, Z., Sharshir, S. (2014). Mathematical and experimental investigation of a solar humidification-dehumidification desalination unit. *Desalination*, 358, 9-17. https://doi.org/10.1016/j.desal.2014.12.005

Kabeel, A. E., El-Said, E. M. (2013). Applicability of flashing desalination technique for small scale needs using a novel integrated system coupled with nanofluid-base solar collector. *Desalination*, 333(1), 10-22. https://doi.org/10.1016/j.desal.2013.11.021

Kang, H., Yang, Y., Chang, Z., Zheng, H., Duan, Z. (2014). Performance of a two-stage multi-effect desalination system based on humidification-dehumidification process. *Desalination*, 344, 339-349. https://doi.org/10.1016/j.desal.2014.04.004

Lavanga, V., Farné, S. (2016). Method and device for the homogeneous and delimited mixing of fluids. Patent n. 102015902343234. Pubblication number WO2016092579

Lavanga, V., Farné, S. (2017). Method for the continuous desalinization and device for the implementation of said method. Patent n. 0001427399. Pubblication number WO2016162896

Lavanga, V., Sparacino, A. C. (2013). Termopozzo. Patent n. 0000275666. Publication Number MI20130148.

Li, X., Yuan, G., Wang, Z., Li, H., Xu, Z. (2014). Experimental study on a humidification and dehumidification desalination system of solar air heater with evacuated tubes. *Desalination*, 351, 1-8. https://doi.org/10.1016/j.desal.2014.07.008

Magrini, A., Magnani, L. (2009). *Fisica Tecnica: Volume 1 - Esempi di calcolo di termodinamica e trasmissione del calore*. Torino: CittàStudi Edizioni.

Moran, M., Shapiro, H., Munson, B., DeWitt, D. (2011). *Introduction to thermal systems engineering*. New York: McGraw Hill

Nam, W. K., Seockheon, L., Dooil, K., Seungkwan, H., Ji, H. K. (2011). Analyses of calcium carbonate scale deposition on four RO membranes under a seawater desalination condition. *Water Science and Technology*, 64(8), 1573-1580. https://doi.org/10.2166/wst.2011.671

Nematollahi, F., Rahimi, A., Gheinani, T. T. (2013). Experimental and theoretical energy and exergy analysis for a solar desalination system. *Desalination*, 317, 23-31. https://doi.org/10.1016/j.desal.2013.02.021

Pantani, R. (2010). *Effetti termici nelle trasformazioni*. Principi di ingegneria chimica ambientale, Università di Salerno, Dipartimento di Ingegneria Industriale, Salerno.

Park, G. L., Schafer, A. I., Richards, B. S. (2012). The effect of intermittent operation on a wind-powered membrane system for brackish water desalination. *Water Science and Technology*, 65(5), 867-874. https://doi.org/10.2166/wst.2012.912

Qiblawey, H. M., & Banat, F. (2008). Solar thermal desalination technologies. *Desalination*, 220(1-3), 633-644. https://doi.org/10.1016/j.desal.2007.01.059

Reddy, S., Sharon, H. (2014). *A review of solar energy driven desalination technologies*. New York: Elsevier.

Rognoni, M. (2010). *La dissalazione dell'acqua di mare. Descrizione, analisi e valutazione delle principali tecnologie*. Palermo, Italy: Dario Flaccovio Editore.

Salata, F., Coppi, M. (2014). A first approach study on the desalination of sea water using heat transformer powered by solar ponds. *Applied Energy*, 136, 611-618. https://doi.org/10.1016/j.apenergy.2014.09.079

Clarkson, C. R. (1998). The effect of coal composition, moisture content, and pore volume distribution upon single and binary gas equilibrium and nonequilibrium adsorption: implications for gas content determination (Doctoral dissertation, University of British Columbia).

Tzen, E., Zaragoza, G., Alarcòn Padilla, D. C. (2012). Solar Desalination. *Comprehensive Renewable Energy*, 3, 529-565. https://doi:10.1016/B978-0-08-087872-0.00316-4

World Health Organization. (2017) Guidelines for drinking-water quality, United Nations, Geneva.

Yildirim, C., Solmus, I. (2014). A parametric study on a humidification-dehumidification desalination unit powered by a solar air and water heaters. *Energy Conversion and Management*, 86, 568-575. https://doi.org/10.1016/j.enconman.2014.06.016

489 Tables

490

491 Table 1. Plants powered by solar panels (Tzen et al., 2012)

Name of the plant	Solar panel (m^2)	Fresh water ($m^3\ d^{-1}$)
Lampedusa (Italy) MSF plant	408	7.2
San Luiz de paz (Mexico)	354	10
El Paso (Texas) MSF plant	3355	19
Abu Dhabi (EAU) MED plant	1862	120
Lampedusa (Italy) MSF plant	500	72

492

493 Table 2. Operating conditions of the SDGC system

Total pressure inside the tank	Pa	30,000.00
Average saltwater temperature in steady state (free surface)	°C	60.00
Humidified air temperature	°C	60.00
Dehumidified air temperature	°C	30.00
Total evaporating surface	m^2	16.74
Humid air speed	$m\ ^{s-1}$	9.00

494 Table 3. Power loss from the tank

Wall stratigraphy			
Layer	Thickness	Conductivity	Transmittance
	m	$W\ m^{-1}\ K^{-1}$	$W\ m^{-2}\ K^{-1}$
External conductive coefficient	//	//	25.00
Stiferite GT	0.1	0.023	0.23
Stiferite GT	0.1	0.023	0.23
CLS concrete	0.1	1.600	16.00
Vertical wall (air/air)			
Internal conductive coefficient	$W\ m^{-2}\ K^{-1}$		8.00
Total thermal transmittance	$W\ m^{-2}\ K^{-1}$		0.11
Total surface	m^2		19.02
Horizontal wall – Ascending flux (air/air)			
Internal conductive coefficient	$W\ m^{-2}\ K^{-1}$		9.30
Total thermal transmittance	$W\ m^{-2}\ K^{-1}$		0.11
Total surface	m^2		21.39
Vertical wall (air/water)			
Internal conductive coefficient	$W\ m^{-1}\ K^{-1}$		800.00
Total thermal transmittance	$W\ m^{-2}\ K^{-1}$		0.11
Total surface	m^2		34.80
Ground dispersion			
Ground type	type		sand/gravel
Ground conductivity	$W\ m^{-2}\ K^{-1}$		2.00
Heat capacity per unit of volume	$kJ\ m^{-3}\ K^{-1}$		2000.00
Specific size (area / perimeter)	m		1.84
Total thickness of external perimeter walls	m		0.30
Internal surface thermal resistance	$m^2\ K\ W^{-1}$		0.0013
Equivalent thickness	m		0.38
Thermal transmittance	$W\ m^{-2}\ K^{-1}$		1.80
Total surface	m^2		21.39
Power losses from the tank			
Average annual outdoor temperature (Milan, Italy)	°C		13.00
Average internal temperature	°C		35.00
Power loss	kW		1.03

Table 4. Total water flow

Physical state of water on the free surface		
Hygrometric degree	//	1.00
Saturation pressure	Pa	19,943.76
Partial vapor pressure	Pa	19,943.76
Physical state of dehumidified water		
Kinematic viscosity	$m^2 s^{-1}$	0.0000162
Hygrometric degree	//	1.00
Saturation pressure	Pa	4246.03
Partial vapor pressure	Pa	4246.03
Other data		
Specific size	m	0.90
Binary diffusion at the process conditions	$m^2 s^{-1}$	0.0000974
Adimensional number		
Reynolds	//	500,000.00
Schmidt	//	0.17
Sherwood (laminar flux)	//	258.23
Evaporated water flow		
Conveying material transport coefficient	$m s^{-1}$	0.0279
Flow of water evaporated from one half of the tank	$kg s^{-1}$	0.0232
Total evaporated water flow	$kg s^{-1}$	0.0464
	$kg d^{-1}$	4012.09
Latent heat of vaporization at operating conditions	$kJ kg^{-1}$	2362.37
Thermal power transferred	kW	109.70

Table 5. Primary heat exchanger sizing

Operating temperature		
Delivery temperature	°C	75.00
Return temperature	°C	45.00
Piping		
Outer diameter	mm	32.00
Thickness	mm	1.50
Internal diameter	mm	29.00
Operating data		
Volumetric flow rate exchanger - half tank	$m^3 h^{-1}$	3.57
Total volumetric flow	$m^3 h^{-1}$	7.13
Flow		
Reynolds	//	500,000.00
Schmidt	//	0.17
Sherwood (laminar flux)	//	258.23
Heat exchanger (half tank)		
Step (distance between two contiguous hole centres)	$m MU^{-1}$	0.082
Number of passes approximated down	MU	10.00
Estimated pipe length	m	93.00
Power transmissible		
Thermal power transmissible from the single exchanger	kW	124.42

Table 6. Condensing power

Hygrometric condition

Specificy humidity - humidified air	$g_v\ kg_{as}^{-1}$	1240.00
Specific humidity - dehumidified air	$g_v\ kg_{as}^{-1}$	102.80
Condensate production		
Amount of specific condensate	$g_v\ kg_{as}^{-1}$	1137.20
Air flow needed		
Mass flow of dry air	$kg\ s^{-1}$	0.04
	$kg\ h^{-1}$	147.00
Partial pressure of dry air	Pa	10,056.24
Dry air specific constant	$J\ kg^{-1}\ K^{-1}$	287.00
Mass flow of moist air	$kg\ s^{-1}$	0.39
	$kg\ h^{-1}$	1397.05
Condensing power		
Enthalpy moist air - humidified air	$kJ\ kg^{-1}$	3300.00
Enthalpy moist air - dehumidified air	$kJ\ kg^{-1}$	293.00
Enthalpy of condensed	$kJ\ kg^{-1}$	125.79
Condensation power	**kW**	**-116.95**

498 Table 7. Thermal tunnel sizing

Presumed temperature at the base of the thermal tunnel	°C	20.00
Convective coefficient at the base of the tunnel	$W\ m^{-2}\ K^{-1}$	3149.20
Reduction hypothesis due to the insulating overlap	%	30.00
Presumptive convective coefficient	$W\ m^{-2}\ K^{-1}$	944.76
Thermal conductivity of aluminum	$W\ m^{-1}\ K^{-1}$	210.00
Expanded metal commercial surface	m^2	2.00
Equivalent metal surface	m^2	1.54
Fin length	m	0.80
“m" coefficient of the fin	m^{-1}	67.07
“A” coefficient of the fin	K	-40.00
“B" coefficient of the fin	K	0.00
Specific thermal flow	$kW\ fin^{-1}$	-0.90
Number of fins	fin	15.00

499 Table 8. Kloben Sky Pro 18

Optical efficiency	%	71.80
Opening surface	m^2	3.43
Absorption surface	m^2	4.65
Heat loss - 1st order	$W\ m^{-2}\ K^{-1}$	1.051
Heat loss - 2nd order	$W\ m^{-2}\ K^{-1}$	0.004

500 Table 9. Solar collectors sizing

Energy losses from the tank		
Hours of operation per year	$h\ year^{-1}$	8000.00
Annual energy loss	$kWh\ year^{-1}$	8276.80
Solar radiation on inclined surface		
Location	//	Milan
Azimuth	°	0.00
Inclination with respect to the horizontal plane	°	35.00
Reflection coefficient on the ground	//	0.20

Shadows and obstacles	//	none
Global radiation on inclined surface	kWh m^{-2} $year^{-1}$	1612.00
Irradiation on inclined surface	W m	184.02
Solar collectors operating efficency		
Thermal medium fluid temperature	°C	60.00
Average annual room temperature	°C	13.00
Collector operational efficiency	%	40.15
Solar collectors' numbers		
Effective radiation absorbed by the collector	kW h m^{-2} $year^{-1}$	647.29
Exchange surface required	m^2	12.79
Number of collectors - opening surface	//	4.00
Number of collectors - absorption surface	//	3.00
Numbers of solar collectors	//	4.00

501 Table 10. Heat-pump generator datasheet

Performance data - EN 14511		
Operating conditions	//	W10/W35
Useful power	kW	28.10
Refrigeration power	kW	23.70
Electric power absorbed	kW	4.73
Performance coefficient (COP)	//	5.94
Primary circuit (evaporator)		
Capacity	l	6.50
Minimum volumetric flow rate	L h^{-1}	5200.00
Loss of load	kPa	17.00
Maximum flow temperature (ground circuit input)	°C	25.00
Minimum flow temperature (ground circuit input)	°C	7.50
Solar collectors' numbers		
Effective radiation absorbed by the collector	kW h m^{-2} $year^{-1}$	647.29
Exchange surface required	m^2	12.79
Number of collectors - opening surface	//	4.00
Number of collectors - absorption surface	//	3.00
Numbers of solar collectors	//	4.00
Secondary circuit (condenser)		
Capacity	l	6.50
Minimum volumetric flow rate	L h^{-1}	1900.00
Loss of load	kPa	3.80
Maximum flow temperature	°C	60.00

502 Table 11. Heat pump generator - operating conditions

Energy requirements		
Saltwater temperature at the entrance	°C	15.00
Operating temperature for heat pump	°C	55.00

Specific saltwater heat	kJ kg^{-1} K^{-1}	3.93
Saltwater density	kg m^{-3}	1025.00
Mass to be heated	kg	5147.55
Thermal energy to be supplied	kWh	224.49
Heat pump - operating conditions		
Thermal power yield	kW	24.92
Performance coefficient (COP)	//	3.68
Electric power absorbed	kW	6.77
Hours of operation		
Time needed to join the full capacity	h	9.01

503 Table 12. Secondary heat exchanger (upper/lower)

Fresh water data		
Delivery temperature	°C	20.00
Minimum return temperature	°C	50.00
Average temperature	°C	35.00
Thermal conductivity at average temperature	W m^{-1} K^{-1}	0.62
Kinematic viscosity at average temperature	m^2 s^{-1}	7.52E-07
Piping data		
Estimated length	m	9.30
Outer diameter	mm	50.00
Thickness	mm	1.00
Internal fluid speed	m s^{-1}	2.50
Material conductivity	W m^{-1} K^{-1}	390.00
Conductive resistance	K W^{-1}	1.79E-06
Internal convective heat resistance		
Prandtl	//	5.04
Reynolds	//	159,574.47
Nusselt - turbulent flux in heating	//	638.57
Internal convective coefficient	W m^{-2} K^{-1}	8242.88
Internal convective heat resistance	K W^{-1}	8.65E-05
External convective heat resistance		
Film temperature	K	320.5
Kinematic air viscosity at the film temperature	m^2 s^{-1}	1.77E-05
Thermal conductivity at the film temperature	W m^{-1} K^{-1}	0.02754
Reynolds	//	25,359.26
Prandtl	//	0.7099
Nusselt - laminar flow	//	102.0706701
External convective coefficient	W $m^{-2}K^{-1}$	56.22
External convective thermal resistance	K W^{-1}	1.22E-02
Power		
Total thermal resistance	K W^{-1}	1.23E-02
Thermal power absorbed	kW	3.26
Number of installations	exchangers	15.00
Potential for total exchange	kW	48.92

504 Table 13. Secondary heat exchanger (left/right)

Fresh water data		
Delivery temperature	°C	20.00

Minimum return temperature	°C	50.00
Average temperature	°C	35.00
Thermal conductivity at average temperature	$W\ m^{-1}\ K^{-1}$	0.62
Kinematic viscosity at average temperature	$m^2\ s^{-1}$	7.52E-07
Piping data		
Estimated length	m	18.60
Outer diameter	mm	50.00
Thickness	mm	1.00
Internal fluid speed	$m\ s^{-1}$	2.50
Material conductivity	$W\ m^{-1}\ K^{-1}$	390.00
Conductive resistance	$K\ W^{-1}$	8.96E-07
Internal convective heat resistance		
Prandtl	//	5.04
Reynolds	//	159,574.47
Nusselt - turbulent flux in heating	//	638.57
Internal convective coefficient	$W\ m^{-2}\ K^{-1}$	8242.88
Internal convective heat resistance	$K\ W^{-1}$	4.33E-05
External convective heat resistance		
Film temperature	K	320.50
Kinematic air viscosity at the film temperature	$m^2\ s^{-1}$	5.86E-07
Thermal conductivity at the film temperature	$W\ m^{-1}\ K^{-1}$	0.64
Cubic expansion coefficient	K^{-1}	4.37E-04
Grashoff	//	3.90E+07
Prandtl	//	3.76
Rayleigh	//	1.47E+08
Nusselt	//	76.48
External convective coefficient	$W\ m^{-2}\ K^{-1}$	975.20
External convective thermal resistance	$K\ W^{-1}$	3.51E-04
Power		
Total thermal resistance	$K\ W^{-1}$	3.95E-04
Thermal power absorbed	kW	63.27
Number of installations	exchangers	6.00
Potential for total exchange	kW	379.63

505 Table 14. Secondary heat exchanger – validation

Balance temperature	°C	60.00
Operating recovery temperature	°C	20.00
Total mass of water	kg	33,617.95
Mass of water to be cooled	kg	23,532.57
Energy spent on cooling	MJ	3940.29
Prandtl	MWh	1.09
Time spent cooling	h	2.88

506 Table 15. Comparison between SDGC plant and existing technologies (Al-Karaghouli & Kazmerski 2013)

Technology		Typical capacity	Specific consumption		Cost
		$m^3\ d^{-1}$	$kWh_e\ m^{-3}$	$€\ m^{-3}$	$€\ m^{-3}$
Processes of renewable sources	Solar still	< 0.1	1 – 6	//	1 – 6
	Solar MEH	1 – 100	2 – 6	100	2 – 6
	Solar MD	0.15 – 10	8 – 15	150 – 200	8 – 15
	Solar MED	> 5000	1.8 – 2.2	60 – 70	1.8 – 2.2

	PV-RO	< 100	5 – 7	//	5 – 7
	PV-EDR	< 100	8 – 9	//	8 – 9
	Solar still	< 0.1	1 – 6	//	1 – 6
Conventional sources processes	WIND - RO	50 – 2000	3 – 7	//	3 – 7
	MSF	6 – 500	1 – 4	70 – 90	1 - 4
	MED	10 – 200	3 – 10	70 – 90	3 – 10
	RO	10 – 120	3 – 7	//	3 – 7
SDGC		> 4	1 – 3	< 3	< 3

507

508 Table 16. table Technical-economic data of installed systems

Technology - Installation	Size $m^3\ d^{-1}$	Investment €	O & M € $year^{-1}$	Water cost € m^{-3}	Energy req kWh m^{-3}
[5]Solar - HDH*	0.022	1400.00	270.00	0.04–0.089	nd**
[6]Solar - HDH*	0.02	10,775.00	1200.00	156.00	nd**
[7]Solar - HDH*	0.5	11,440.00	80.00	4.15	nd**
[8]ST - MED - Abu Dhabi	120	2,037,783.00	nd**	6.58	50.91
[8]ST - MED - Almeria	73	nd**	nd**	nd**	3.3 – 5
[8]PV - RO - Lampedusa	120	nd**	nd**	6.5	5.5 - 6
[8]PV - RO - BW - Ceara	8	11,300.00	654.00	10.32	4.7
[8]PV - RO-Pozo Izquierdo	3.2	nd**	nd**	9	5.5
SDGC	150	1,087,160.24	45,702.31	0.90	1.82
*prototype; **undeclared					

[5] Hamed et al., 2014
[6] Bacha, 2013
[7] Chang et al., 2014
[8] Tzen et al., 2012

509

Figures

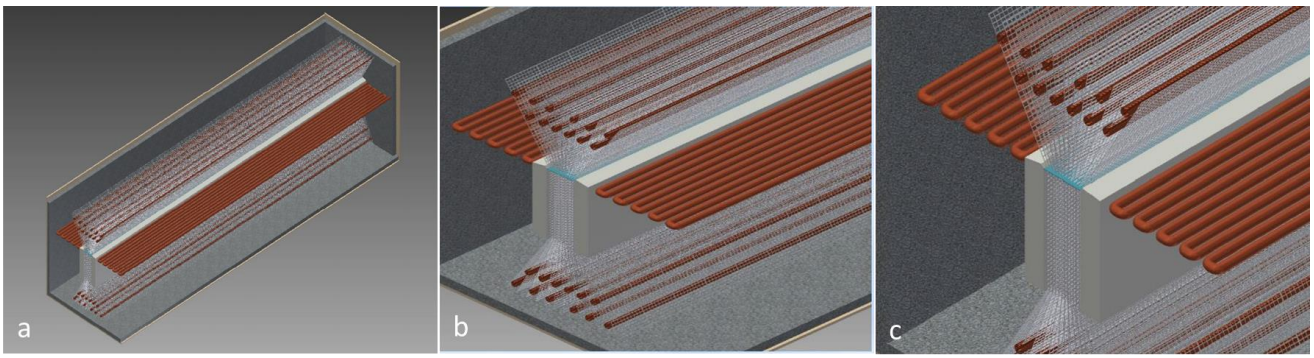

Figure 1. Perspective view (a) and details (b and c) of the SDGC device

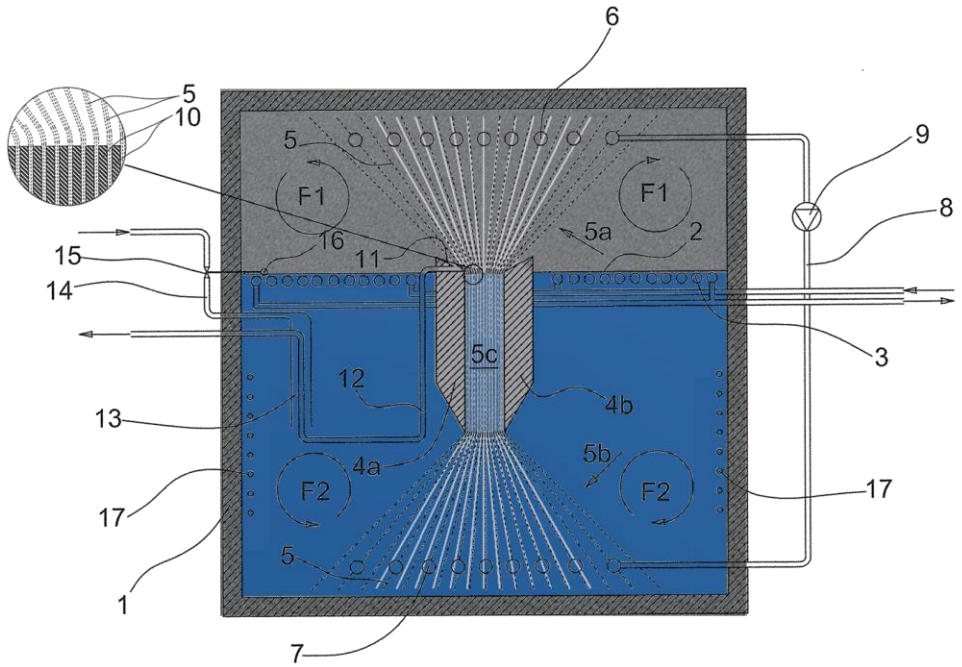

Figure 2. Section of the SDGC device, obtained by a transverse plane. F1 and F2 convective motions; 1 tank, 2 water level; 3-6-7-13-17 heat exchangers; 4a and 4b bars; 5 (a, b, c) metal sheets; 8-12-14 pipes; 9 pump; 10 sealant; 11 reservoir; 15 valve; 16 level relief device

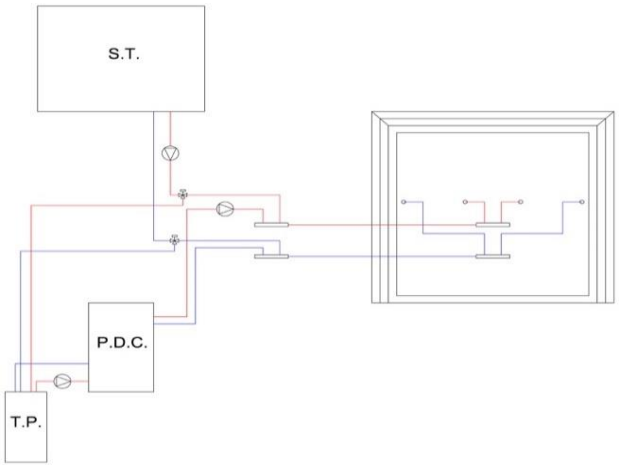

Figure 3. Solar Desalination Geothermal assisted Continuous simplified plant layout with the heat generators: solar thermal (S.T.), heat pump (P.D.C.) and thermo-well (T.P.).

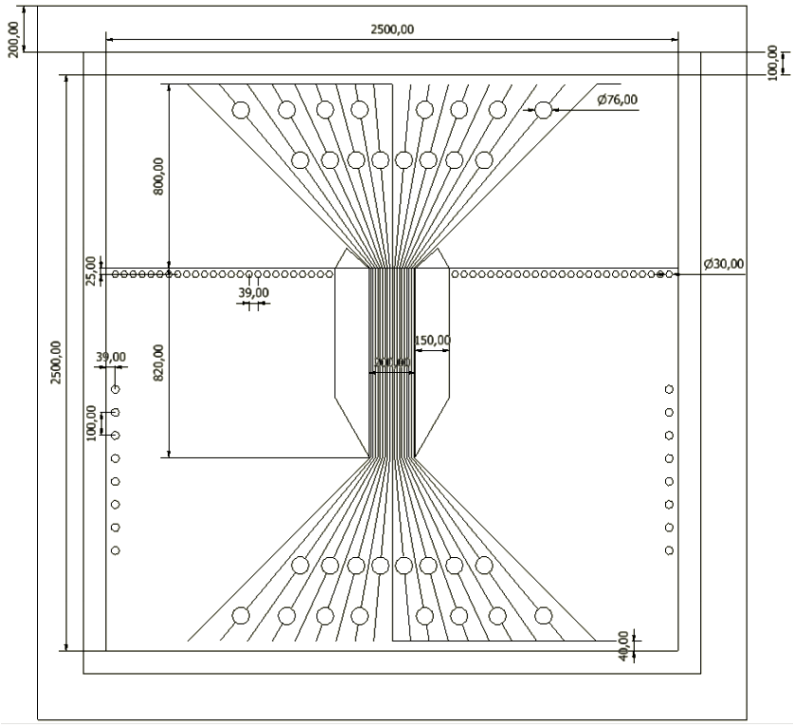

Figure 4. SDGC case study drawing with the main dimensions